571 APPLICATIONS OF RADAR-DERIVED SHEAR PRODUCTS USING AN UPDATED LINEAR LEAST-SQUARES DERIVATIVE TECHNIQUE

Matthew C. Mahalik
Cooperative Institute for Mesoscale Meteorological Studies, The University of Oklahoma, and
NOAA/OAR/National Severe Storms Laboratory, Norman, Oklahoma

1. Introduction

The Linear Least-Squares Derivative (LLSD; Elmore 1994) method is an approach to calculating gradients across two-dimensional (2D) radar data. Mathematically, an LLSD gradient is represented by the slope of the least-squares plane fit to a neighborhood of data points. Operational products created in the LLSD framework first pass input radar data through a median filter (Huang et al. 1979), producing a more continuous and "smooth" field to analyze. LLSD itself then works to mitigate effects of random noise remaining in the data by considering surrounding gates.

The LLSD governing equations (included as a system in the Appendix) form the basis of the azimuthal (rotational) shear (AzShear; Smith and Elmore 2004) product within the National Severe Storms Laboratory (NSSL) Multi-Radar Multi-Sensor (MRMS) system (Smith et al. 2016). As part of an effort to improve the accuracy of AzShear, the LLSD equations were re-derived and corrected for previous simplifying assumptions (Mahalik et al. 2016). The result is a complete and mathematically sound set of equations for calculating 2D gradients in a radial data field. The system has the capability to incorporate dynamic scanning strategies such as Supplemental Adaptive Intra-Volume Low-Level Scan (SAILS; Chrisman 2013).

While (at the time of this work) it is operationally applied only to the development of AzShear products, the relative accuracy and flexibility of LLSD allows it to be applied to a wide variety of radar data products. This paper presents several examples of how LLSD may be applied to radar data and explores the utility of the resulting products, many of which remain in an experimental state. All examples herein were developed using the NSSL Warning Decision Support System-Integrated Information (WDSS-II; Lakshmanan 2007) developmental software and National Weather Service Weather Surveillance Radar-1988 Doppler (WSR-88D) data but can also be applied to radar data from other sources.

Corresponding Author Address: Matthew C. Mahalik, OU/CIMMS NOAA/NSSL, National Weather Center, 120 David L. Boren Blvd., Norman, OK 73071;
E-mail: matthew.mahalik@noaa.gov

2. Across-Azimuth Shear

The azimuthal component of the LLSD technique is essentially a method of numerically estimating the vertical vorticity equation for the radial component of the wind; as such, when calculated across an azimuth, it yields one-half of the total vertical vorticity (ζ; Eq. 1), or "half-vorticity," under the assumption of local symmetry.

$$\zeta = \frac{\partial v}{\partial x} - \frac{\partial u}{\partial y} \quad (1)$$

The slope of the best-fit plane across the radial (corresponding to ∂x) neglects the along-azimuth (∂y) component such that only the first term of Eq. 1 remains, resulting in an expression for half-vorticity. This term, the component of the radial velocity (v_r) derivative across azimuth θ, can be expressed as u_θ. This calculation is repeated across the entire radial velocity field, always along a radial but with the neighborhood shifting around the radar site. While this procedure strictly produces half-vorticity, the term "AzShear" is used interchangeably here since the final product has been established by that name.

AzShear is a popular product used to detect rotation. Weak signatures and other non-obvious circulations in the traditional radial velocity display are often much more easily identified when examining an AzShear field (Fig. 1).

3. Along-Azimuth Shear

The same LLSD equations used to calculate rotational component of shear can be solved for the along-azimuth shear component. This process is similar to AzShear calculations, but the slope of the best-fit plane is instead computed along the azimuth, range-wise. Mathematically, this is the radial component of the derivative of v_r, written as u_r, yielding an expression for 2D radial half-divergence (positive) and half-convergence (negative). The resulting product is referred to as LLSD divergent shear (DivShear). A wide range of information can be gleaned by examining this data. Examples for several different storm modes follow.

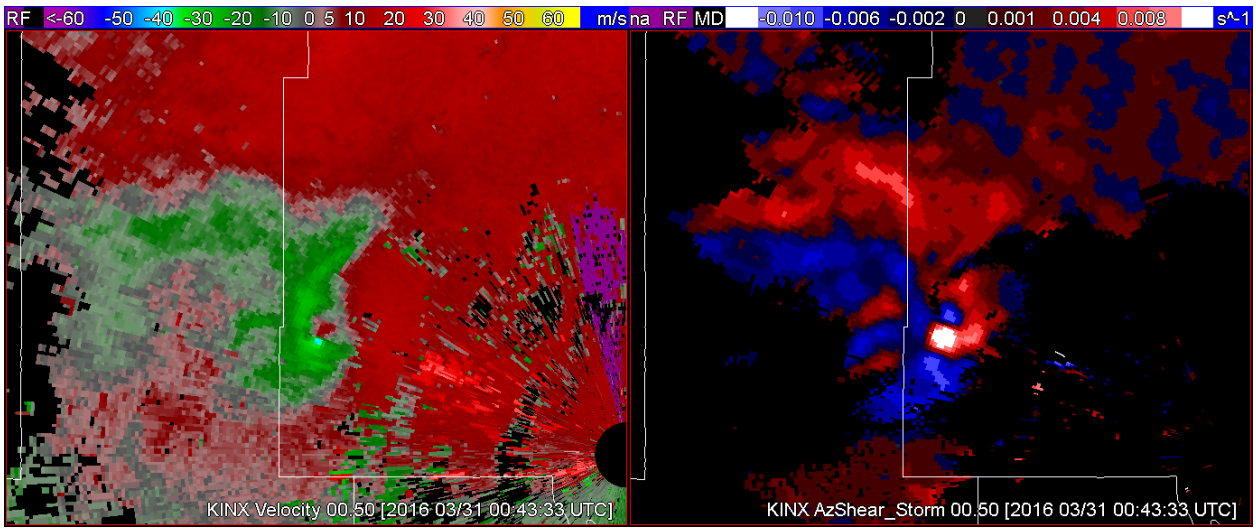

***Fig. 1**. 0.5° dealiased Doppler velocity (left) and 0.5° AzShear (right) depiction of a tornadic supercell on 30 Mar 2016 near Tulsa, OK. The low-level mesocyclone is highlighted as a maximum in AzShear (white). AzShear values exceeded the upper bounds of the color table in this case.*

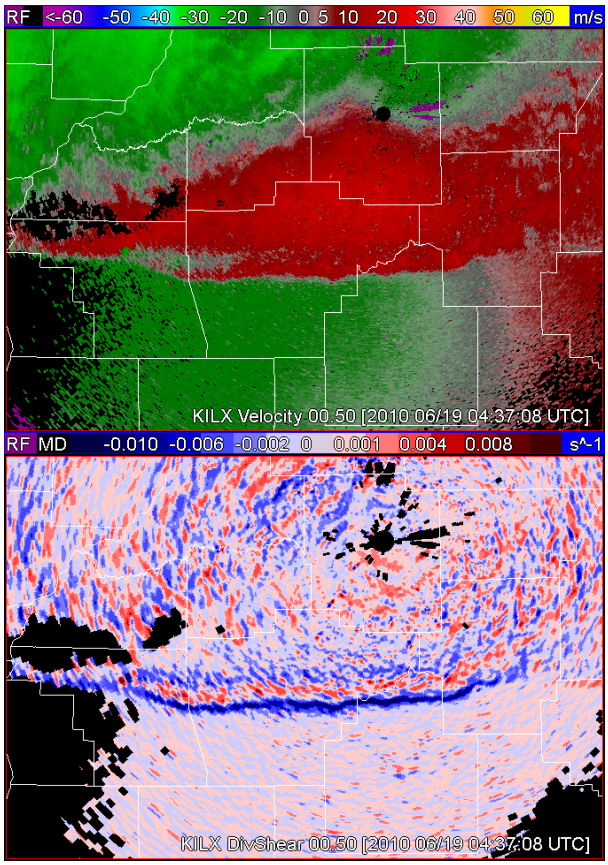

***Fig. 2**. 0.5° dealiased Doppler velocity (top) and 0.5° Divergent Shear (bottom) depiction of a southward-moving gust front on 18 Jun 2010 in Central Illinois. The gust front appears as strong convergence (blue).*

3a. Gust Fronts/Convergence Lines

Gust fronts are mainly long, narrow regions of convergence at the leading edge of advancing, often rain-cooled air and are occasionally associated with strong, damaging wind gusts. LLSD DivShear highlights these features as elongated regions of strongly negative divergence. Figure 2 shows an example of such a gust front that resulted in severe, damaging wind gusts across parts of Iowa, Illinois, and Indiana on 18 Jun 2010. The DivShear field not only shows the presence of a convergence boundary represented by large negative values. Gust fronts can also be associated with significant vertical vorticity, but DivShear measurements may be used to help differentiate them from rotational features. In addition, smaller-scale features in the velocity field not obvious in the radial velocity field are apparent, including a wavelike pattern behind the initial gust front and a more heterogeneous field behind the front, indicating a more turbulent, gusty flow near the ground.

The example shown here is a clear, large squall line feature, but other convergence boundaries can be detected as well, such as thunderstorm outflow gust fronts, sea and land breeze boundaries, and dry lines, among others, which are often the focus of convective initiation.

3b. Supercells

DivShear could also be used to interrogate small-scale structure of airflow within supercell thunderstorms. For example, a classic tornadic supercell is shown in Figure 3, and several well-

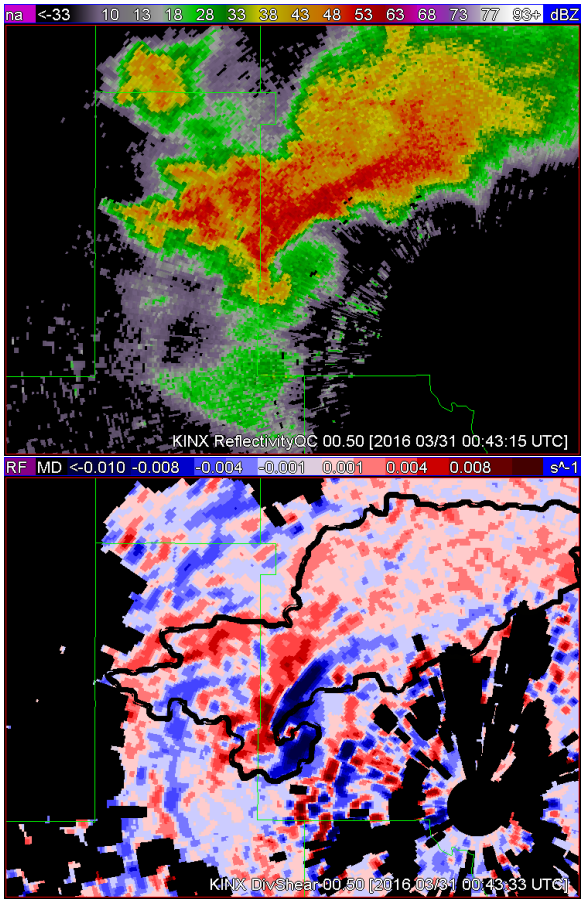

Fig. 3*. 0.5° Reflectivity (top) and 0.5° Divergent Shear (bottom, with 25 dBZ reflectivity contour in black) depiction of a tornadic supercell on 30 Mar 2016 near Tulsa, OK.*

known supercellular features are identifiable. Most obvious are areas of strong convergence occurring along the southeastern flank of the storm and a region of strong divergence within the core of the storm.

Along the leading edge of the reflectivity hook, the convergence may represent the leading edge of the rear-flank gust front. An additional area of strong convergence directly north of the hook may signify the convergence boundary. North of the hook, the region of strong convergence may represent the forward flank convergence boundary (Beck and Weiss 2013).

Divergence is commonly observed within precipitation cores, as it signals downdrafts (such as those induced by negative buoyancy and precipitation drag) reaching the surface; in this case, the divergence immediately west of the reflectivity hook may be associated with the rear-flank downdraft (RFD). Interestingly, a small area of divergence near the surface can be seen in Figure 2 co-located with the EF2 tornado that was occurring at the time. More examples must be studied before any definitive statement can be made about the appearance of tornadoes in a DivShear field. It also remains unclear how decreasing horizontal resolution affects the ability to resolve these features.

3c. Downbursts

One of the original motivations for calculating LLSD shear was to detect damaging downburst signatures, which have significant ramifications in operational and aviation meteorology (Smith et al. 2003). A downburst is defined as a thunderstorm downdraft that produces a sudden outflow of horizontal wind at the surface (Fujita 1981). DivShear can be leveraged to detect common characteristics of downbursts. Typically, a strong downburst appears as a region of strong divergence near the surface as the sinking air reaches the ground and spreads radially. This is usually preceded by convergence aloft as mass converges and descends (Roberts and Wilson 1989).

Figure 4 shows an example of a damaging downburst generated by a typical thunderstorm in Florida. The low-level (0.5° elevation) scan clearly shows the divergence maximum associated with the downburst (the outflow boundary that initiated the convection as it drifted westward is also apparent as a narrow, elongated convergence feature). At higher altitude, strong convergence is evident at the same location in the preceding 10° elevation scan. In this case, the low-level radial velocity looks fairly unremarkable, but the DivShear field clearly highlights areas of interest. This shows the utility of gradient products that may be able to pick out features not otherwise obvious in the velocity field. These radial convergence characteristics are commonly observed in such damaging downbursts (like those discussed by Roberts and Wilson 1989) and the ability to detect them using 2D DivShear field could assist in future development of an automated downburst detection algorithm.

4. Reflectivity Gradients

While the majority of work to develop LLSD shear calculations has focused on radial velocity scans, the technique can also be applied to non-velocity radar products. For example, reflectivity gradients can be derived by applying the same equations but replacing v_r with reflectivity (Z). When the resulting along- and across-azimuth gradients are added, the end product is the total, absolute gradient of reflectivity. This has the effect of producing a reflectivity “stencil,” outlining individual storms or multicell clusters. The product highlights any sharp changes in reflectivity, which themselves are caused by a myriad of meteorological phenomena. For example, a large tornado “debris ball”, an important part of the tornado debris signature

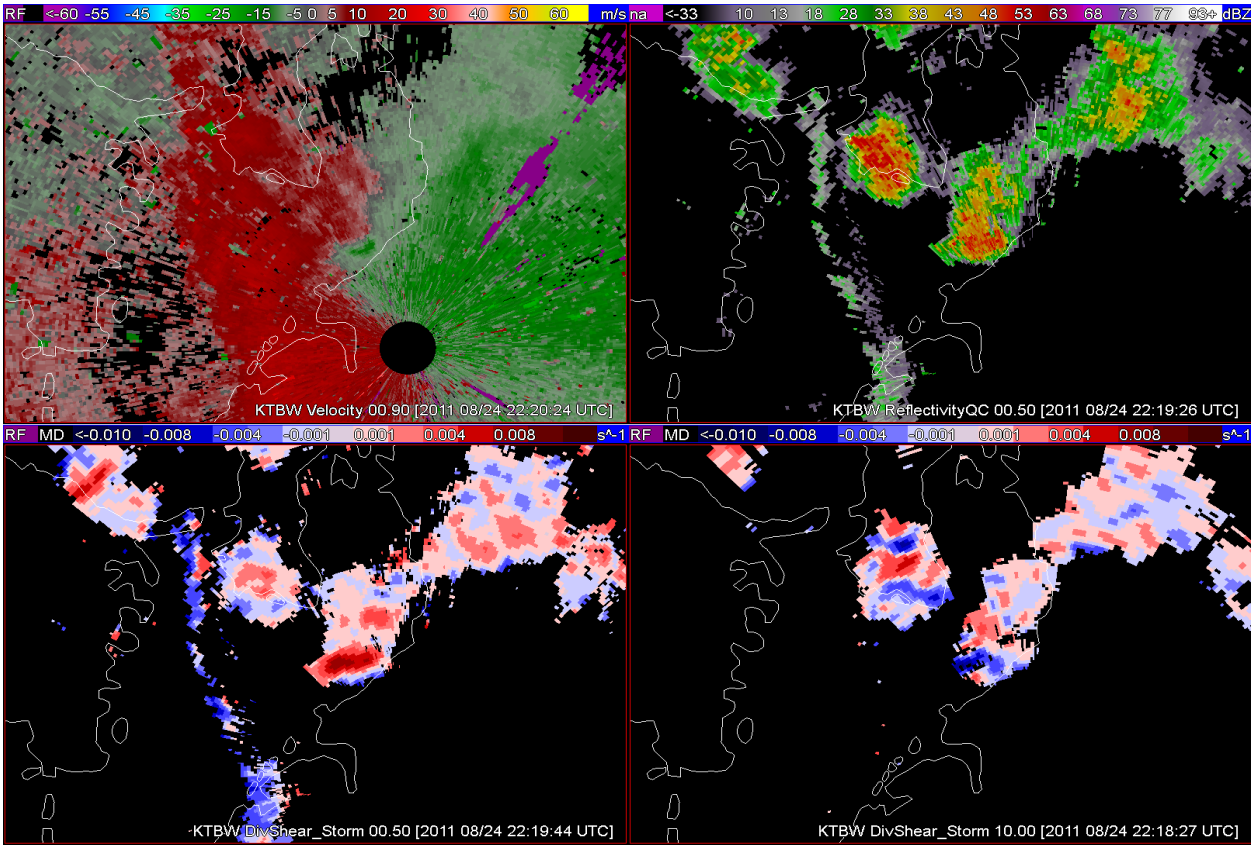

Fig. 4. *Clockwise from top-left: 0.9° dealiased Doppler velocity, 0.5° Reflectivity, 10.0° Divergent Shear, and 0.5° Divergent Shear depiction of a damaging downburst and outflow boundary on 24 Aug 2011 near Tampa, FL. The downburst is collocated with strong divergence (red) near the ground and convergence (blue) aloft.*

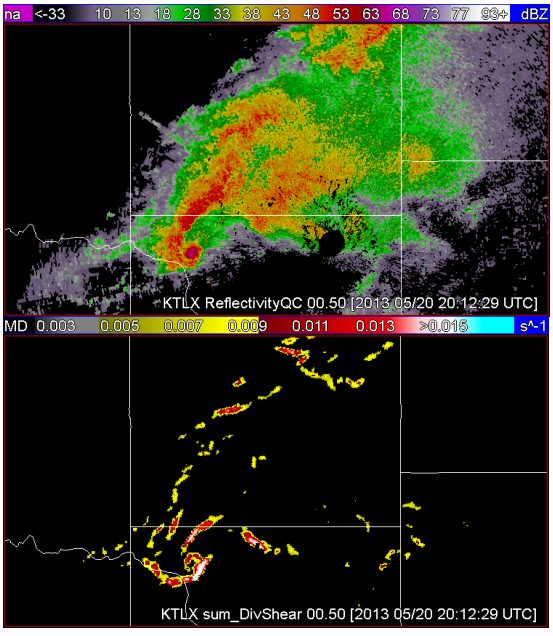

Fig. 5*. 0.5° Reflectivity (top) and corresponding LLSD reflectivity gradient ("stencil") depiction (bottom) of a tornadic supercell on 20 May 2013 near Moore, OK.*

(Ryzhkov et al. 2005), is essentially a reflectivity maximum. As shown in Figure 5, a well-defined, isolated debris ball will have a notable reflectivity gradient surrounding it; thus it is visualized as a hollow circle of large gradients. However, this pattern is not easily discernable when a tornado is embedded heavy precipitation and is surrounded by additional high reflectivity.

Although the utility of reflectivity gradient calculations has yet to be explored in depth, this type of product may be useful in future storm classification or pattern recognition efforts, for example.

5. Summary and Future Work

The examples shown here are a first look at applications of the LLSD governing equations beyond traditional rotational shear products. The purpose of this discussion is to provide an update on ongoing work to improve existing LLSD shear products and explore potential future products leveraging the LLSD framework. It is stressed that the products described here exist in their preliminary stage.

Although the technique is more tolerant of noisy data than many other methods of calculating 2D fields

of radar variable gradients, the ultimate accuracy of any algorithm based on LLSD is subject to the quality of input radar data. Another consideration is that, as with most radar-based quantities, LLSD products tend to have a range-based bias, where values change at greater distances from the radar due to lower resolution from beamspreading. This problem is well-documented for LLSD AzShear (Mahalik et al. 2016; Newman et al. 2013), but its effects on DivShear and other gradient calculations have yet to be examined quantitatively.

In addition to a thorough exploration of possible failure points, a quantitative analysis of the overall performance of these products, including a determination of the optimal neighborhood size for divergence calculations, will follow. Traditionally, LLSD AzShear is calculated using an approximately constant window measuring 2500 m x 750 m, but an additional analysis must be performed to determine the optimal neighborhood size for other quantities.

Future work will include expanding LLSD implementation over spectral width and dual-polarization variable fields. Ultimately, the gradient fields shown here are designed for wider use in a variety of future applications, including detection, tracking, and trending algorithms. In addition, output from LLSD algorithms can add value to ongoing analyses. For example, updated LLSD AzShear will serve as the basis of a nationwide climatology of low- and midlevel storm rotation as part of the Multi-Year Reanalysis of Remotely Sensed Storms (MYRORSS; Cintineo et al. 2012, Ortega 2015).

6. Acknowledgements

Recognition is deserved for colleagues working on various LLSD-related projects, particularly Brandon Smith, Travis Smith, Kim Elmore, Darrel Kingfield, and Kiel Ortega. Funding for this provided by NOAA/Office of Oceanic and Atmospheric Research under NOAA-University of Oklahoma Cooperative Agreement #NA11OAR4320072, U.S. Department of Commerce. The statements, findings, conclusions, and recommendations are those of the author(s) and do not necessarily reflect the views of NOAA or the U.S. Department of Commerce.

7. References

Beck, J., and C. Weiss, 2013: An assessment of low-level baroclinity and vorticity within a simulated supercell. *Mon. Wea. Rev.* **141**, 649-669.

Chrisman, J. N., 2013: Dynamic Scanning. *Radar Operations Center NEXRAD Now,* **22**, 1-3. [Available online at *http://www.roc.noaa.gov/WSR88D/PublicDocs/NNOW/NNow22c.pdf*.]

Cintineo, J., T. Smith, V. Lakshmanan, and S. Ansari, 2011: An automated system for processing the Multi-Year Reanalysis of Remotely Sensed Storms (MYRORSS). Preprints, *27th Conf. on Interactive Information Processing Systems (IIPS),* Seattle, WA, Amer. Meteor. Soc., J9.3.

Elmore, K. M., E. D. Albo, R. K. Goodrich, and D. J. Peters, 1994: NASA/NCAR airborne and ground-based wind shear studies. Final Rep., Contract NCC1-155, 343 pp.

Fujita, T. T., 1981: Tornadoes and downbursts in the context of generalized planetary scales. *J. Atmos. Sci.*, **38**, 1511-1534.

Huang, T., G. Yang, and G. Tang, 1979: A fast two-dimensional median filtering algorithm. *IEEE Trans. Acoust., Speech, Signal Process.*, **27**, 13-18.

Lakshmanan, V., T. Smith, G. Stumpf, and K. Hondl, 2007: The warning decision support system–integrated information. *Wea. Forecasting*, **22**, 596-612.

Mahalik, M. C., B. R. Smith, D. M. Kingfield, K. L. Ortega, T. M. Smith, and K. L. Elmore, 2016: Improving NSSL Azimuthal Shear Calculations Using an Updated Derivation and Range-Based Corrections. *28th Conf. on Severe Local Storms*, Portland, OR, Amer. Meteor. Soc., 182.

Newman, J. F., V. Lakshmanan, P. L. Heinselman, M. B. Richman, and T. M. Smith, 2013: Range-correcting azimuthal shear in Doppler radar data. *Wea. Forecasting*, **28**, 194-211.

Ortega, K. L., 2015: A radar-based storm climatology for the contiguous United States for improved severe weather climatologies and warnings. *31st Conf. EIPT*, Phoenix, AZ, Amer. Meteor. Soc., 10.3.

Roberts, R. D., and J. W. Wilson, 1989: A proposed microburst nowcasting procedure using single-Doppler radar. *J. Appl. Meteor. Climatol*, **28**, 285-303.

Ryzhkov, A. V., T. J. Schuur, D. W. Burgess, & D. S. Zrnic, 2005: Polarimetric tornado detection. *J. Appl. Meteor.*, **44**, 557-570.

Smith, T. M., and K. L. Elmore, 2004: The use of radial velocity derivatives to diagnose rotation and divergence. Preprints, *11th Conf. on Aviation, Range, and Aerospace*, Hyannis, MA, Amer. Meteor. Soc., P5.6.

Smith, T. M., K. L. Elmore, and S. A. Dulin, 2003: A damaging downburst prediction and detection algorithm for the WSR-88D. *Wea. Forecasting*, **19**, 240-250.

Smith, T. M., and coauthors, 2016: Multi-Radar Multi-Sensor (MRMS) severe weather and aviation products: Initial operating capabilities. *Bull. Amer. Meteor. Soc.*, **97**, 1617–1630.

Appendix

Linear-Least Squares Derivative (LLSD) Governing Equations

$$\sum_{i=0}^{n} u_{ij} w_{ij} \Delta r_i = \sum_{i=0}^{n} u_0 w_{ij} \Delta r_i + \sum_{i=0}^{n} u_r w_{ij} (\Delta r_i)^2 + \sum_{i=0}^{n} u_\theta w_{ij} \Delta r_i \Delta \theta_{ij}$$

$$\sum_{i=0}^{n} u_{ij} w_{ij} \Delta \theta_{ij} = \sum_{i=0}^{n} u_0 w_{ij} \Delta \theta_{ij} + \sum_{i=0}^{n} u_r w_{ij} \Delta r_i \Delta \theta_{ij} + \sum_{i=0}^{n} u_\theta w_{ij} \Delta r_i (\Delta \theta_{ij})^2$$

$$\sum_{i=0}^{n} u_{ij} w_{ij} = \sum_{i=0}^{n} u_0 w_{ij} + \sum_{i=0}^{n} u_r w_{ij} \Delta r_i + \sum_{i=0}^{n} u_\theta w_{ij} \Delta \theta_{ij}$$

These three equations can be expressed in matrix form as follows, where all summations are over *i*=0 to *i*=*n*. From here, the system can be solved for the rotational (u_θ) and divergent (u_r) shear components.

$$\begin{bmatrix} \Sigma \Delta r_i^2 & \Sigma \Delta r_i \Delta \theta_{ij} & \Sigma \Delta r_i \\ \Sigma \Delta r_i \Delta \theta_{ij} & \Sigma \Delta \theta_{ij}^2 & \Sigma \Delta s_{ij} \\ \Sigma \Delta r_i & \Sigma \Delta \theta_{ij} & \Sigma\, 1 \end{bmatrix} \begin{bmatrix} u_\theta \\ u_r \\ u_0 \end{bmatrix} = \begin{bmatrix} \Sigma \Delta r_i u_{ij} \\ \Sigma \Delta \theta_{ij} u_{ij} \\ \Sigma u_{ij} \end{bmatrix}$$

List of Variables

i, j - range and azimuth index for each kernel grid point

n - number of grid points in the LLSD kernel

Δr_i – range distance from center of LLSD kernel

$\Delta \theta_{ij}$ – azimuthal distance from center of LLSD kernel

u_r – Across-azimuth component of Doppler radial velocity

u_θ – Radial component of Doppler radial velocity

u_0 – Non-physical term for the remaining component of Doppler radial velocity

u_{ij} – Doppler radial velocity measurement at kernel grid point (i, j)

w_{ij} - local weight at kernel grid point (i, j)